Contents lists available at ScienceDirect

Solar Energy Materials & Solar Cells

Grain size dependence of degradation of aluminium/calcium cathodes in organic solar cells following exposure to humid air

T.S. Glen [a], N.W. Scarratt [b], H. Yi [c], A. Iraqi [c], T. Wang [b], J. Kingsley [d], A.R. Buckley [b], D.G. Lidzey [b], A.M. Donald [a],*

[a] University of Cambridge, Cavendish Laboratory, J J Thomson Avenue, Cambridge CB3 0HE, United Kingdom
[b] University of Sheffield, Department of Physics and Astronomy, Hicks Building, Hounsfield Road, Sheffield S3 7RH, United Kingdom
[c] University of Sheffield, Department of Chemistry, Dainton Building, Brook Hill, Sheffield S3 7HF, United Kingdom
[d] Ossila Limited, Kroto Innovation Centre, Broad Lane, Sheffield S3 7HQ, United Kingdom

ARTICLE INFO

ABSTRACT

Cross-sectional TEM and SEM have been used to study the degradation of organic solar cells when exposed to a high humidity environment. Two obvious effects were caused by this exposure: voids at the aluminium/calcium interface and large bubble like protrusions on the top surface. Water ingress was found to occur mainly from the edge rather than through pinholes or defects in the aluminium film. The grain size of the aluminium used in the cathode was varied and small grained devices were found to have degraded faster. The importance of minimising water ingress into devices through cathode design and choice of materials is highlighted.

1. Introduction

Organic materials can potentially provide cheap, flexible, thin film solar cells that are easily manufactured in large volumes and contain no hazardous materials [1,2]. However, organic photovoltaic (OPV) devices still have low efficiencies compared with other materials and have lifetime problems due to sensitivity to ultraviolet light, water and oxygen [3,4]. Whilst a lot of work has been directed towards increasing efficiencies, the longevity and operational performance over time of these devices are just as important and is a growing area of interest in the field.

Degradation of OPV performance is complex and cannot be described by a single process. This is mainly due to the multi-layered structure and finely balanced morphology of the active layer. Lifetimes for unencapsulated devices are often a day or less. Encapsulation techniques can improve that considerably, but add additional costs and processing stages [5,6].

Much previous work has focused on monitoring the electrical performance of devices over time [7–9], with some observing the effect of exposure to different environments [10–12]. This is useful in that it provides quantitative values and practical parameters that can be seen to worsen. However it is not straightforward to separate the various causes of degradation and to identify which, if any, are dominant. Different techniques are needed in conjunction in order to understand all of the different degradation mechanisms and hence interpret the decreased lifetime.

One study used air exposure at various stages of device fabrication to determine which layer is being affected by air [13]. When tested, samples in which organic layers were previously exposed to air showed no difference to freshly made devices. It was thus concluded that the measured increase in series resistance with time as devices were aged was due to the oxidation of the aluminium at the aluminium/active layer interface. Using impedance spectroscopy it was proposed that this layer of aluminium oxide acts as a charge-blocking layer and grows thicker with time.

Another study used X-ray photoelectron spectroscopy (XPS) depth profiles to show the presence of aluminium oxide at the interface after ageing and that the use of PEDOT:PSS as the hole transport layer led to faster formation of this oxide layer, as well as faster degradation of the device performance [14].

Stability measurements have been made on devices with various cathodes and exposures [15]. Strong evidence was found that changes at the metal/active layer interface can account for a significant amount of the total loss of efficiency. These studies show

---

* Corresponding author.
  E-mail address: amd3@cam.ac.uk (A.M. Donald).

the importance of the cathode/active layer interface in organic solar cells.

The first reports of 'bubbles' forming in cathodes of organic devices came in the 90s in work on organic light emitting diodes (OLEDs) [16–18]. These bubbles were attributed to electrochemical reactions with water and oxygen, producing hydrogen and oxygen, which became trapped and caused delamination of the layers of the device.

Cross-sectional transmission electron microscopy (TEM) has previously been used to study degradation in OPVs. Thermal annealing has been used to drive phase separation and consequent growth of the P3HT:PCBM active layer into elongated protrusions [19], which were observed and studied using cross-sectional TEM alongside other techniques. It was found that these protrusions were formed from the lateral diffusion of the active layer and that the metal cathode remained intact until over 100 h of annealing.

The same technique has also been used to study the aluminium/active layer interface and an intermixed layer of ~3 nm was reported [20]. It was argued that this could not be an oxide layer as the devices were fabricated in a nitrogen glovebox, contrary to similar TEM work done on deposited aluminium films [21]. However, an intermixing layer of 2 nm at an aluminium/P3HT interface was also reported by another group using X-ray reflectivity [22]. Clearly there is some doubt regarding the details of this interface.

Small holes, or 'voids', at an aluminium/calcium interface have been previously reported [23]. In this study devices were kept in the dark and performance was monitored before cross-sectional TEM images were taken. Relatively stable open circuit voltage (V_{oc}) and a sharp drop in the short circuit current density (J_{sc}) combined with the TEM images suggested that the observed voids were the main cause of degradation in device performance with calcium and aluminium cathodes. These were thought to have been caused by oxygen and water, which are thought to ingress through grain boundaries and pinholes present in the cathode [24,25].

Another study found that water ingress was significant from both pinholes and from the edge of devices [26]. They also found that the rate of degradation was quicker at the edge of devices than around even large pinholes, but edge effects could be reduced by appropriate lateral design of the device. Indeed, it was found that if the cathode extended beyond the active area the degradation was significantly reduced.

Water diffusion from the edges through the PEDOT:PSS layer has been linked with the oxidation of the cathode and loss of J_{sc} [27]. By replacing the cathode on aged devices the J_{sc} could be fully recovered. The use of alternative hole transport layers was also found to reduce the observed degradation.

Recently, an adapted calcium test was used to measure the water ingress into non-encapsulated small molecule solar cells [28]. The calcium test is described in detail elsewhere [29]. It was found that most of the water ingress was through macroscopic defects in the aluminium top layer, and a few large (radius >300 nm) defects contributed to most (>72%) of the permeation. It has been argued that water is the primary source of degradation in devices [4,28].

We have studied the exposure of OPV devices to high humidity air. Unencapsulated devices have been exposed to humid air in order to accelerate any possible damage caused by water ingress. The use of a dual-beam Focussed Ion Beam–Scanning Electron Microscope (FIB-SEM) allows fabrication of cross-sectional site specific TEM samples. These TEM images obtained showed both large scale bubble defects and also smaller voids at the cathode-polymer interface.

The grain size of the evaporated aluminium used in the cathode was varied by changing the rate of deposition. This has been shown

to change the rate of degradation, which, to our knowledge, is an effect which has not been previously reported.

It was found that degradation at the cathode interface is the cause of device failure in humid conditions, and have proposed the formation of voids at the interface as a key degradation mechanism. Water ingress and dependence on the grain size of the aluminium used in the cathode was explored.

This work links previously reported void formation [23] with water ingress and used electron microscopy to confirm ingress from the edges of devices [26] and to view the effects of water on the cathode and PEDOT:PSS in operational devices.

2. Experimental

2.1. Device fabrication

OPV devices were fabricated on pre-patterned indium tin oxide (ITO) substrates provided by Ossila Ltd. The size of the substrates used was 20×15 mm, with six active pixels of 4 mm^2 on each. The substrates were cleaned by sonication; first with a Hellmanex® solution, then dilute sodium hydroxide (NaOH) and finally isopropyl alcohol.

The polymer used in the active layer for this study was poly[N-9′-heptadecanyl-2,7-carbazole-alt-5,5-(4′, 7′-di-2-thienyl-2′, 1′, 3′-othiadiazole)], known as PCDTBT, synthesised by Yi as reported previously [30]. The electron acceptor used was [6,6]-phenyl-C$_{71}$ butyric acid methyl ester (PC$_{70}$BM), provided by Ossila Ltd. The active layer was dissolved in a polymer:PC$_{70}$BM ratio of 1:4 at a concentration of 8 mg/ml in chlorobenzene.

The architecture of devices was ITO/PEDOT:PSS/PCDTBT-PC$_{70}$BM/calcium/aluminium, as shown in the schematic in Fig. 1. The PEDOT:PSS was spun cast onto ITO patterned substrates in air to form a layer ~20 nm thick before being annealed for 5 min at 130 °C to remove absorbed moisture. The PCDTBT-PC$_{70}$BM active layer was spun cast in a nitrogen glovebox to form a layer ~70 nm thick. The PEDOT:PSS and active layer were then wiped off the cathode ITO contact using chlorobenzene and a cotton bud.

The cathode was thermally evaporated using the chamber in the glovebox. A ~8 nm thick layer of calcium was deposited by evaporation followed by ~75 nm of aluminium. The aluminium grain size was varied between devices by changing the rate of deposition. A rate of ~1 nm/s was found to give large grains, whilst ~0.01 nm/s was used for small grain films. Grain size was measured using a TEM to image the top surface of grains deposited onto a TEM grid placed alongside devices in the evaporator. The area of the large grains was measured at 6900 ± 2000 nm^2, whilst the slower rate produced grains of 110 ± 10 nm^2, where the errors are the standard error of the mean. Figs. S1–S4 show TEM images
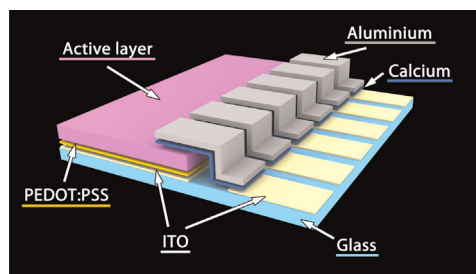
Fig. 1. Organic photovoltaic device structure. Photocurrent is collected at the aluminium/calcium cathode or at the ITO anode. This strip of aluminium/calcium is later referred to as a 'stripe', and connects the active area to another ITO contact for ease of electrical connection. The spin coated PEDOT:PSS and active layer are wiped away from the ITO connecting with the cathode. The active region of the device is the part with all the layers present, shown in the middle.

of small and large grain films. Finished devices were left unencapsulated and sealed in the glovebox for transportation to be aged or tested.

Two batches of devices were fabricated. One batch was used to record the change in J–V characteristics after devices were aged in a high humidity environment. The other was used to provide devices that were cross-sectioned and viewed using electron microscopy at various stages of ageing.

2.2. Device ageing

Devices were aged in high humidity by placing them in a desiccator with a saturated salt solution. Sodium acetate ($C_2H_3NaO_2$) was used to give a relative humidity of 76% [31], and devices were placed in this for an hour before being removed and tested again. This was repeated for 4 h, before being left overnight and tested again after a total of 15 h.

2.3. Electron microscopy

SEM images of the top surfaces were taken using an FEI Philips Dualbeam Quanta 3D FIB. Images were taken at 10 kV. Cross-sectional TEM samples were prepared using the in situ liftout method described in detail in the supporting information and elsewhere [32]. Samples had a thickness ~70 nm or less as determined using the SEM of the dual-beam system. Once completed, specimens for TEM imaging were then transferred immediately to an FEI Philips Tecnai 20 and viewed at 200 kV.

Cross-sectional SEM images were taken at 5 kV using the FIB tomography or 'slice and view' technique, described in detail in the supporting information, with a Zeiss Crossbeam. This was undertaken several days after the devices were aged and TEM samples prepared. During this period the devices were stored in a vacuum desiccator.

Where possible, cross-sections were taken from several places in the operational area of the solar device. On aged samples, cross-sections were taken both from visibly degraded and apparently intact areas.

ImageJ software was used to measure the area of voids seen in cross-sectional TEM images. Where possible, four images of different areas across two different cross-sections per device type were used, and the areas of all the voids measured. In this way an average and error was obtained.

2.4. Device testing

To obtain their J–V characteristics devices were illuminated under a Newport 9225 1A-1000 AM1.5 solar simulator, under ambient conditions with the use of a shadow mask to define the active area as 2.12 mm^2. An NREL calibrated silicon cell was used
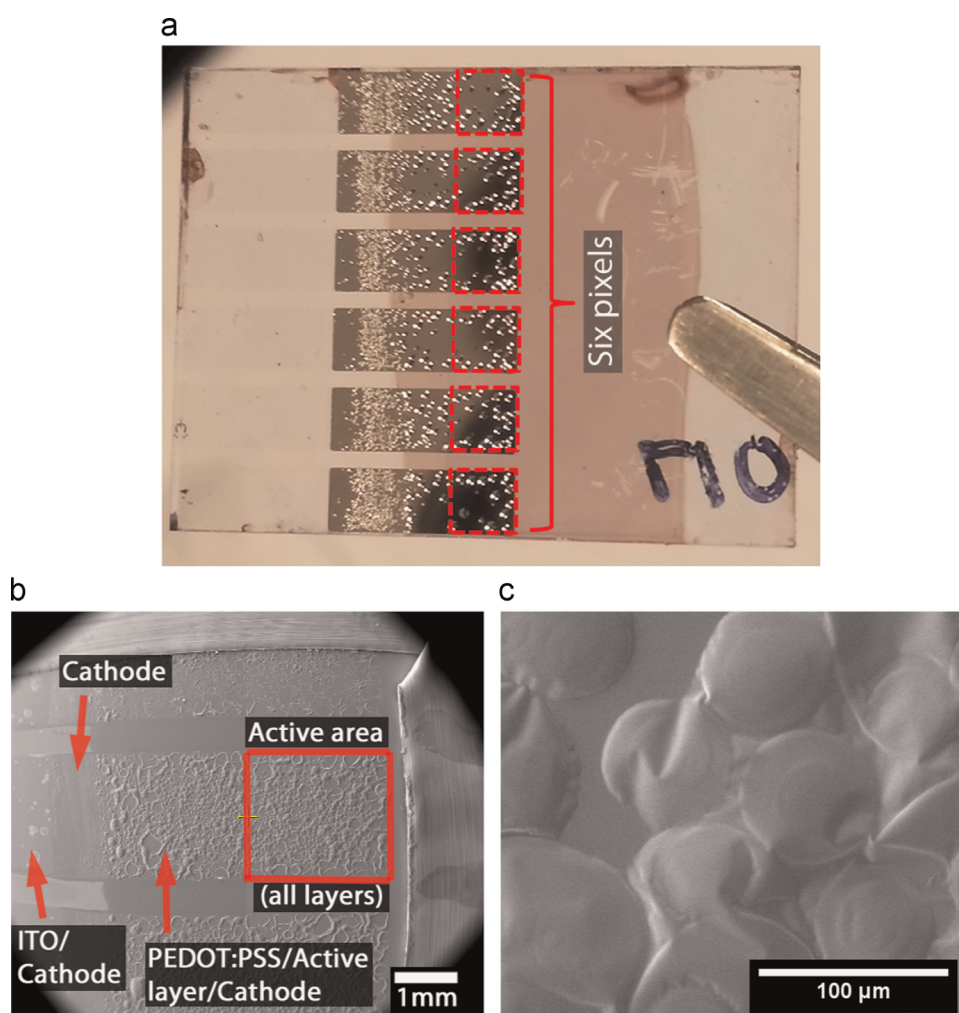
Fig. 2. (a) Photograph of a typical aged device, showing visible damage to the aluminium stripes after 4 h in 76% humidity. Shown in (b) and (c) are top-down SEM images showing similar defects on a device aged for one day in 98% relative humidity. (b) shows how the defects vary across the different regions of the device, whilst (c) is a higher magnification image of the active area and shows the bubble-like structure of the defects.

to calibrate the power output to 100 mW cm^{-2} at 25 °C. A Keithley 237 source meter was used to measure the current as a function of voltage. To eliminate the effect of dead pixels, only the 50% of pixels with the highest performance were used when averaging.

3. Results and discussion

3.1. Bubble defects

Some of the degradation of organic solar cells caused by exposure to high humidity is visible by eye (Fig. 2(a)). The aluminium cathode exhibited shiny spots which, upon closer inspection using the SEM of the dual-beam system, were revealed to be bubble-like protrusions similar to those previously reported [16,18]. In a preliminary investigation, the number of these features was highest on samples aged in ~98% relative humidity for one week, which was the longest ageing period used in this study. These bubbles were not observed on fresh samples – all fresh samples had a smooth top surface. The regions not covered by the cathode showed no visible change, either by eye or when viewed using the SEM.

The average area of the 'bubbles' found in the pixels was measured using the SEM as 9000 ± 1000 µm^2. Further microscopy work, discussed in more detail later, revealed the bubbles consist of a delamination between layers with a clear vertical protrusion on the order of several microns. This is opposed to other degradation effects seen exclusively at the aluminium/calcium interface, which are of a considerably smaller scale and are referred to in this paper as 'voids'.

The bubble defects can be prevalent on aged devices, sometimes covering >70% the area of a pixel. Fig. 2(c) shows a top down SEM image of a highly degraded cell, with several bubbles that have merged together and covered most of the viewed area.

The composition of the device varies at different points across the aluminium/calcium stripe (see Fig. 1), and this has an effect on the size and number of bubbles, as shown in Fig. 2(b). This shows that some of the layers other than those in the cathode are involved in the formation of the bubbles. Fig. 2(b) is a top-down view of the schematic view shown in Fig. 1.

The region in which all the layers are present is shown in Fig. 2(b). At the other end of the aluminium/calcium stripe, no polymer layers are present and the only layers present are aluminium/calcium and ITO. Between these is an area where the PEDOT:PSS and active layer have been wiped away. This wiping process is done by hand and therefore within this central area there are areas where the aluminium/calcium is directly on top of the glass substrate and others where there is PEDOT:PSS and active layer present.

Large bubbles are clearly seen after the devices were aged in 98% relative humidity, as shown in Fig. 2(b). The largest bubbles and the largest proportion of damaged area are seen when PEDOT:PSS and the active layer are both present (i.e. the active area and the area immediately adjacent), but bubbles are still seen in large numbers even when the only layers are glass/calcium/aluminium.

As Fig. 2 illustrates the damage after even one day of exposure to high humidity can be extensive. As some of the bubble defects appeared to be of the order of microns in height when viewed with the SEM, cross-sections of these were taken close to the edge of the defect. Fig. 3(a) shows a low magnification TEM image of a cross-section taken in this way, with a closer view of the edge in Fig. 3(b). These images show that this protrusion has been caused by swelling of the PEDOT:PSS layer to such an extent that a void has formed in this layer. Areas affected by these large bubbles are unlikely to be contributing to a working solar device. As the active layer and anode are no longer in contact under a bubble, any free charges generated in this region are likely to recombine rather than being extracted from the device. It is also possible that there are buried or unseen changes in the chemical composition of the
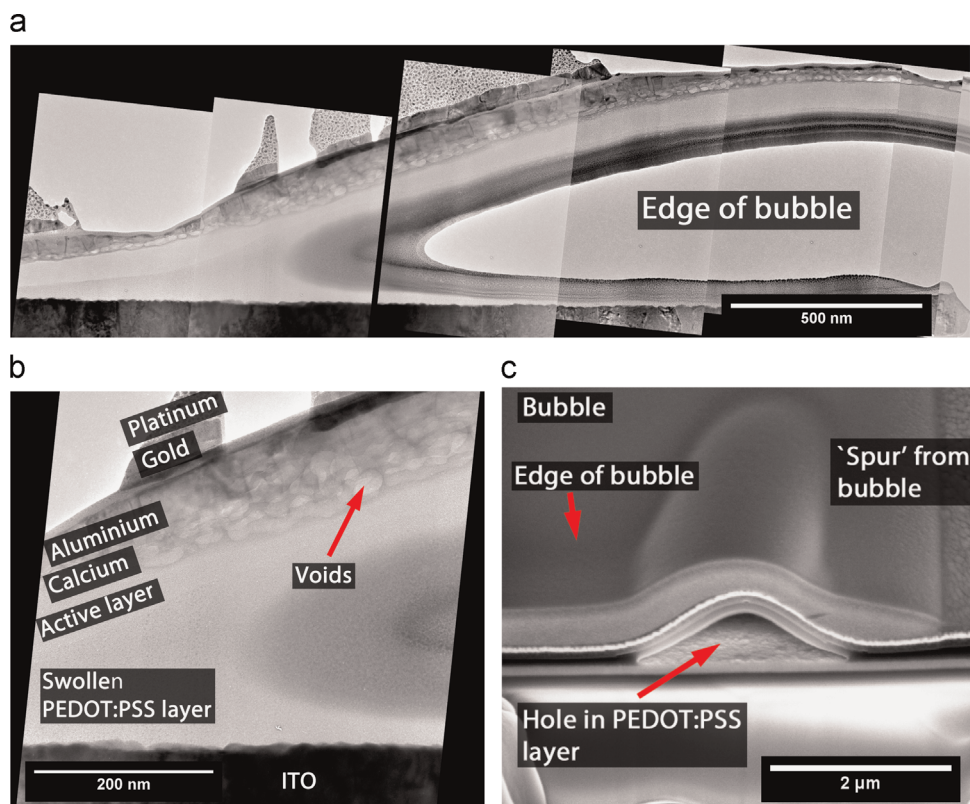
Fig. 3. (a) TEM cross-section through the edge of a bubble, (b) shows the edge of the large defect in (a). A side on SEM image of a slice cut across a 'spur' from one of the larger bubbles is shown in (c).

active layers around a bubble which could affect light absorption or charge transport.

3.2. Void defects

Also visible are extensive, but smaller, voids at the aluminium/calcium interface – most numerous at the site of the bubble defect shown in Fig. 3(b), but present all along the length of the cross-sections taken from this cell. These observations imply that these are probably two different degradation mechanisms although both are potentially caused by water ingress into the device. Similar aluminium/calcium interfacial voids were first reported by Lloyd et al. [23].

Fig. 3(c) was taken from a cell aged for one day in a 98% relative humidity environment. Interlinking protrusions between bubble defects, referred to as 'spurs', were also seen in some devices. Fig. 3(c) shows an SEM image taken after slicing across one of these 'spurs'. Again, it shows that the delamination occurs in the PEDOT:PSS layer, close to the ITO interface. Some of the underlying roughness of the ITO layer can be seen within the hole. Small defects can also be seen at the aluminium/calcium interface at the edge of the PEDOT:PSS protrusion and at the top. These are likely to be caused by the stresses caused by the buckling, especially as this interface is already weakened by the smaller voids that are too small to see with the SEM but have been observed with the TEM and shown in Fig. 3(b).

Fig. 4 shows bright field TEM images highlighting the difference between fresh and aged devices. Contrast in bright field TEM arises from mass-thickness variations. After ageing by exposure to a humid environment, small brighter regions at the aluminium/calcium interface have formed whereas none are observed for fresh samples. As the thickness of the cross-sections are very uniform these brighter regions at the aluminium/calcium interface correspond to less dense regions or voids.

It has been proposed that water ingress occurs through the grain boundaries of the aluminium [23,25]. It is possible that water could accumulate at the aluminium/calcium interface before diffusing through the rest of the device. Both calcium and aluminium react with water at room temperature to produce hydrogen in an exothermic reaction. This reaction and production of hydrogen could be enough to create the voids observed at this interface.

The fact that no swelling or bubbles are observed in the areas of the substrate not covered by the cathode implies that it is not simply caused by the absorption of water. Smaller bubbles are seen with just cathode/ITO/glass and cathode/glass in Fig. 2(c), meaning that the bubbles are formed even without the PEDOT:PSS or active layers present. This suggests that the reactions mentioned above are the cause of the bubbles as well as the voids. If the hydrogen produced cannot escape easily, but can traverse the different layers of the device, then the delamination will occur between the two layers with the least cohesion. This would explain why delamination occurs in the PEDOT:PSS layer (close to the ITO) when present, but still occurs when no polymer layers are present at all. The presence of the PEDOT:PSS layer increases the number and the size of bubbles observed. This could be because of the hygroscopic nature of PEDOT:PSS meaning more water is absorbed into the device, so more hydrogen is produced. The PEDOT:PSS layer could also be swelling as it absorbs water.

The cross-sectional images, such as those in Fig. 4, cannot confirm that water ingress through the grain boundaries is the cause of these voids. Grain boundaries can be identified as darker lines in bright field imaging and can be seen vertically in aluminium layers shown in Fig. 4. Not every grain boundary aligns with a void. This could be explained by some grain boundaries being 'closed' to water ingress if they are too small or well-packed, meaning that water cannot traverse the grain boundary and therefore cannot react at the interface.

Conversely, not every void aligns with an observable grain boundary. This may arise from the nature of taking a cross-section through a sample. If a void is formed at the interface it will be three-dimensional in nature, and therefore it is likely that a thin cross-section could include part of the void but not necessarily the corresponding grain boundary. Alternatively, if water enters the device through the edges and is the cause of the voids, no link with grain boundaries would be expected.

A correlation between the presence of large bubble defects and the smaller voids at the aluminium/calcium interface was observed for aged devices. A slight contrast difference between the 'bubble rich' edge region and the unaffected middle was also observed using SEM and is shown in Fig. 5(a). Cross-sectional TEM images taken from the middle and edge regions show that far more voids are present at the edge.

Fig. 5(b) shows a photograph of a partially degraded device which has had the PEDOT:PSS and active layer removed from the annotated areas before the cathode was deposited. Considering the edge between the regions with and without the polymer layers present (dotted lines in Fig. 5(b)), it can be seen that there are fewer bubbles here compared to the other edges. Either the deposition of the cathode has acted as a crude seal and slowed down the water ingress, or water simply has a longer distance to travel. This is further evidence that edge ingress is more significant than that through pinholes or defects in the aluminium film, as shown by others [26]. The lateral design of a device is important for attempts to reduce degradation caused by water.
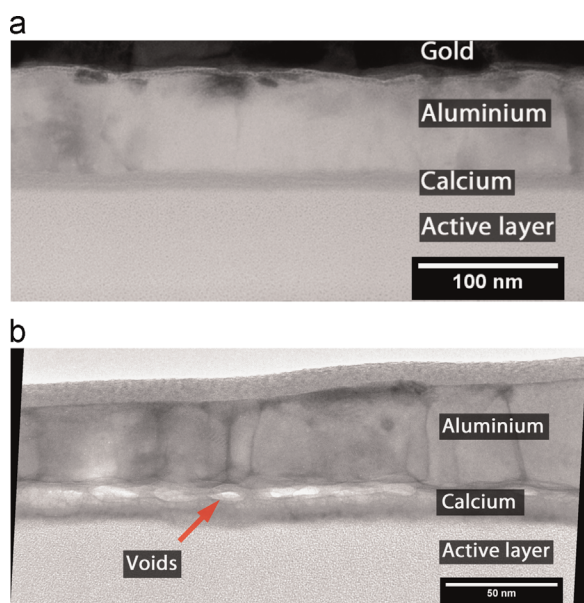
3.3. Aluminium grain size

To explore whether water was able to traverse grain boundaries, the grain size was altered to see if this would produce an observable difference in the amount of degradation. This was done by changing the deposition rate of the thermally evaporated aluminium, as described in the experimental section. An extremely fast deposition rate gave large grains, with fewer grain boundaries. These grain boundaries easily spanned the aluminium layer however, providing a straight path for any penetrating water. An

Fig. 4. TEM images of void formation at the aluminium/calcium interface for aged samples. A typical interface for a fresh device is shown in (a), whilst (b) shows typical void formation at the interface.
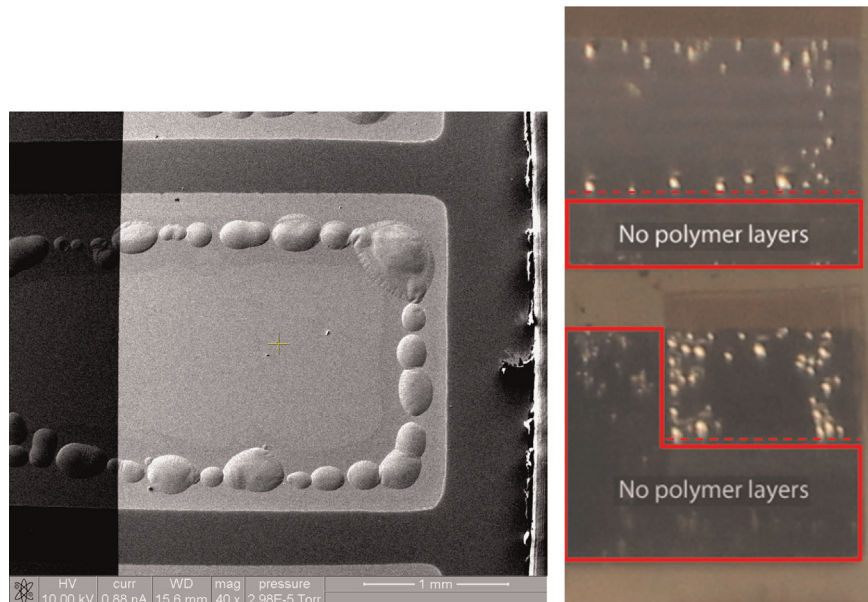
Fig. 5. (a) SEM image showing contrast difference between edge and central regions of the pixel, thought to have been caused by water ingress. (b) Photograph of partial degradation with polymer layers removed from marked areas before cathode deposition. Fewer bubbles can be seen on the bottom edges (dotted lines) where the polymer layers are present.

extremely slow deposition rate gave small grains, with many more grain boundaries. As the typical grain size in this case was smaller than the thickness of the aluminium layer, there was no longer a straight path across the layer through grain boundaries.

More devices were fabricated and imaged after various lengths of time of ageing. Fig. 6 shows a series of low magnification SEM images showing how the degradation varies between devices aged for different times and with different grain sizes. The degradation appears first around the edge of the pixel. Longer degradation times lead to bubbles closer to the middle. This implies that the water ingress from the edges of the device is more important than that through the cathode. Also, fewer bubbles were observed in the small grain devices (right side of Fig. 6).

The area affected by voids was measured and averaged from several TEM images of different areas of devices with different exposure times, and the results are shown in Fig. 7. This graph shows a difference between small grain and large grain devices for cross-sections taken from both the edge and the middle of the pixel. The area affected by voids is larger in devices with small grained aluminium cathodes. Also, the affected area is smaller when cross-sections are taken from the middle of the pixel, as would be expected if water were ingressing from the edges. It should be noted that devices with ~ 60 nm^2 affected by voids had almost the entire sampled area affected.

Comparison with performance is also important. More devices were fabricated so their PCE, J_{sc} and V_{oc} could be measured. Different devices were aged in three different environments and tested periodically as they degraded. Some cells were kept in a 76% relative humidity environment, others were kept in the ambient room conditions, whilst a third group were kept in a dry environment. A clear trend was visible by eye as the devices kept in high humidity suffered from bubble formation after just one hour, whilst those in the dry environment were still mainly visually intact after 14 h.

Fig. 8 shows the change in PCE and J_{sc} as the devices were aged. It is interesting to note that the J_{sc} graph mirrors the PCE graph. The V_{oc} was found to remain fairly constant over the first four hours. Devices left in a dry environment had PCEs over 80% of their initial value after 15 h. Those in ambient humidity had PCEs between 60% and 70% of their initial value depending on the grain size. Devices placed in the
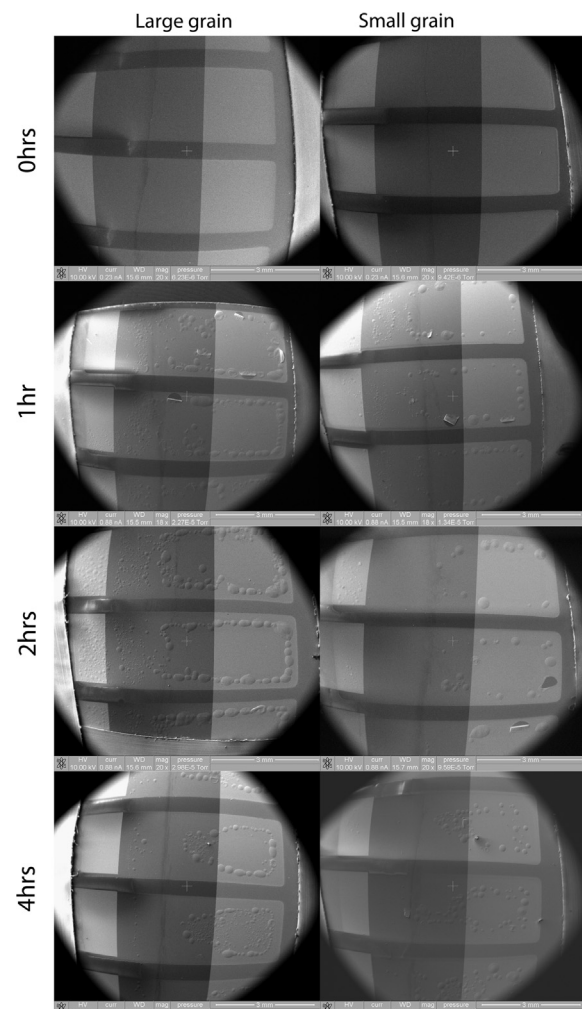
Fig. 6. SEM images showing the early stages of degradation. Left column shows large grained devices, whilst the right column shows small grained. The rows are, from top to bottom, devices aged for 0 h, 1 h, 2 h and 4 h. Bubble defects are seen moving in from the edge of the cathode stripe.

humid desiccator had PCEs 20–30% (again depending on grain size) of their initial value after 4 h, and were no longer functioning after 15 h.
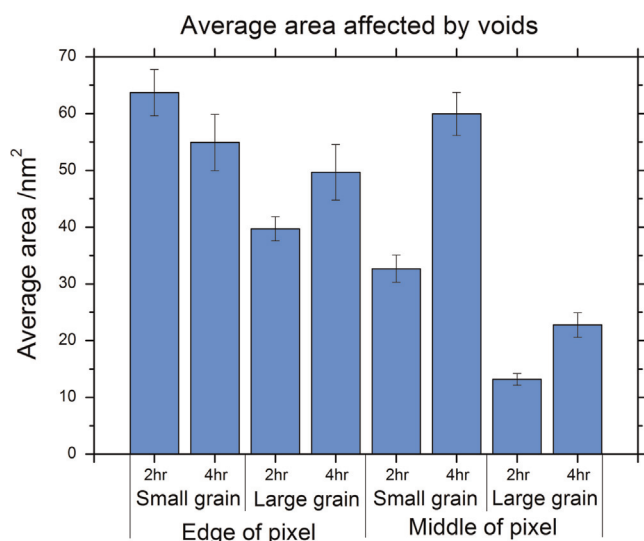
Average area affected by voids

Fig. 7. Average area affected by voids on TEM images from various devices after ageing in 76% relative humidity.
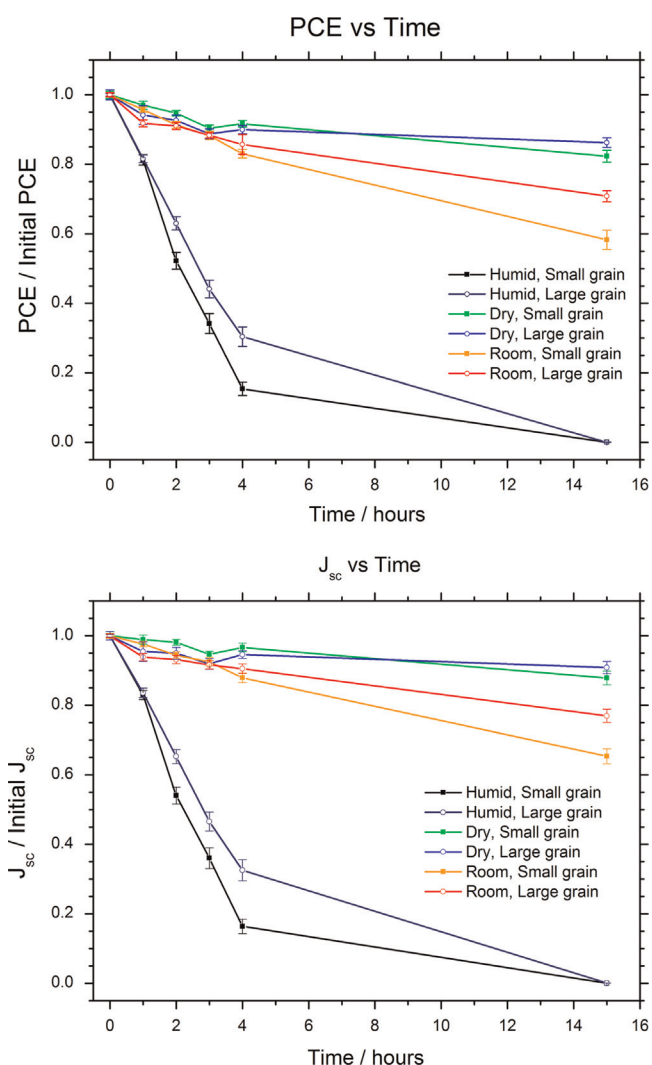

Fig. 8. Graphs showing the decrease in PCE (top) and J_{sc} (bottom). Note initial PCEs were ~5% and initial J_{sc}'s were ~ − 9.5 mA/cm^2

A significant difference was observed between large and small grain devices. After 15 h the small grain devices all had lower normalised PCEs than the large grain devices. The difference is larger in more humid environments.

Our microscopy studies show that fewer bubbles are formed in small grained aluminium devices than in large, whereas voids at the aluminium/calcium interface are prevalent in both. The performance of small grained devices was observed to drop faster than that of large grained devices which suggests that it is the voids that matter and not the bubbles when it comes to performance. The variation in the number of bubbles formed between large and small-grained samples could be due to the differing mechanical properties. Smaller grain size in polycrystalline metals in general leads to higher yield strength [33,34], thereby likely to lead to a greater resistance to bubble formation and a smaller number able to form.

We propose that the (much smaller) voids observed at the aluminium/calcium interface could increase trap assisted recombination [35,36] or simply cause a reduction in contact surface area [23], leading to a decrease in charge extraction from the device. The observed drop in J_{sc}, whilst the V_{oc} remains fairly constant, is consistent with this more difficult charge extraction. However, the exact physical mechanism for this requires further study.

The aluminium/calcium interface is more critical to device performance than the PEDOT:PSS layer. Even with a gap within the PEDOT:PSS as seen in Fig. 3(a), there is little impediment to light reaching the active layer and hence generated photocurrent can still be collected; voids at the aluminium/calcium interface provide recombination sites and prevent charge collection. Therefore the faster degradation of small grain devices can be rationalised: the small grain aluminium film is mechanically less susceptible to bubble formation yet voids still form and cause device failure. The greater susceptibility of devices with small grain aluminium cathodes to voids, as seen in Fig. 7, would therefore lead to faster degradation.

The PEDOT:PSS layer clearly plays a role in the observed degradation, but cannot alone be the cause. Degradation is still observed in regions of the device with no PEDOT:PSS, shown in Figs. 2(b) and 5(b). Also, no bubbles or swelling of the PEDOT:PSS are observed in areas not covered by the cathode. Our work therefore suggests that, by its hygroscopic nature, PEDOT:PSS facilitates and accelerates the degradation caused by the reaction of water with the aluminium/calcium cathode.

Devices in this study were unencapsulated in a high (although not unrealistic) humidity environment to accelerate the ageing process. However, it is worth considering that gradual exposure to small amounts of water over a longer period of time may result in different degradation mechanisms. The results reported here are of interest, but a degree of caution is needed when considering degradation of devices under real-world conditions.

4. Conclusion

This work has shown that water plays an important role in degradation of organic solar cells, with damage on large and small scales to different layers of the device. Clearly the common OPV design of PEDOT:PSS as the hole transport layer and an aluminium/calcium cathode is highly susceptible to degradation in high humidity. Water has been shown to be the cause of bubbles and voids formed within the device. It has been shown that water ingress is mainly from the edge of the device as opposed to through pinholes or defects in the aluminium film. Degradation rate has also been shown to depend on the grain size of the aluminium used in the cathode and linked with void formation at the aluminium/calcium interface, a previously unreported effect which could prove interesting when considering

other cathode designs. A more complicated cathode design, possibly incorporating barrier layers, a mix of different grain sizes or materials could potentially reduce this. This study thus shows the importance of a good encapsulation method for these devices if long operational lifetimes are to be achieved.

Acknowledgements

Appendix A. Supplementary data

Supplementary data associated with this paper can be found in the online version at http://dx.doi.org/10.1016/j.solmat.2015.03.015.

References

[1] C.J. Brabec, N.S. Sariciftci, J.C. Hummelen, Plastic solar cells, Adv. Funct. Mater. 11 (1) (2001) 15–26.
[2] Y. Zhou, C. Fuentes-Hernandez, T.M. Khan, J.-C. Liu, J. Hsu, J.W. Shim, A. Dindar, J.P. Youngblood, R.J. Moon, B. Kippelen, Recyclable organic solar cells on cellulose nanocrystal substrates, Sci. Rep. 3 (2013).
[3] M. Jørgensen, K. Norrman, F.C. Krebs, Stability/degradation of polymer solar cells, Sol. Energy Mater. Sol. Cells 92 (7) (2008) 686–714.
[4] M.P. Nikiforov, J. Strzalka, S.B. Darling, Delineation of the effects of water and oxygen on the degradation of organic photovoltaic devices, Sol. Energy Mater. Sol. Cells 110 (2013) 36–42.
[5] C.H. Peters, I.T. Sachs-Quintana, J.P. Kastrop, S. Beaupré, M. Leclerc, M. D. McGehee, High efficiency polymer solar cells with long operating lifetimes, Adv. Energy Mater. 1 (4) (2011) 491–494.
[6] R. Roesch, K.-R. Eberhardt, S. Engmann, G. Gobsch, H. Hoppe, Polymer solar cells with enhanced lifetime by improved electrode stability and sealing, Sol. Energy Mater. Sol. Cells 117 (2013) 59–66.
[7] R.A. Street, P.P. Khlyabich, B.C. Thompson, Electrical characterization of organic solar cell contact degradation resulting from ambient exposure, Org. Electron. 14 (11) (2013) 2932–2939.
[8] R. de Bettignies, J. Leroy, M. Firon, C. Sentein, Accelerated lifetime measurements of P3HT: PCBM solar cells, Synth. Met. 156 (7–8) (2006) 510–513.
[9] J.A. Hauch, P. Schilinsky, S.A. Choulis, R. Childers, M. Biele, C.J. Brabec, Flexible organic P3HT: PCBM bulk-heterojunction modules with more than 1 year outdoor lifetime, Sol. Energy Mater. Sol. Cells 92 (7) (2008) 727–731.
[10] S.A. Gevorgyan, M. Jørgensen, F.C. Krebs, A setup for studying stability and degradation of polymer solar cells, Sol. Energy Mater. Sol. Cells 92 (7) (2008) 736–745.
[11] M.O. Reese, A.K. Sigdel, J.J. Berry, D.S. Ginley, S.E. Shaheen, A simple miniature controlled-atmosphere chamber for optoelectronic characterizations, Sol. Energy Mater. Sol. Cells 94 (7) (2010) 1254–1258.
[12] V. Turkovic, S. Engmann, D.A.M. Egbe, M. Himmerlich, S. Krischok, G. Gobsch, H. Hoppe, Multiple stress degradation analysis of the active layer in organic photovoltaics, Sol. Energy Mater. Sol. Cells 120 (2014) 654–668.
[13] M. Wang, F. Xie, J. Du, Q. Tang, S. Zheng, Q. Miao, J. Chen, N. Zhao, J.B. Xu, Degradation mechanism of organic solar cells with aluminum cathode, Sol. Energy Mater. Sol. Cells 95 (12) (2011) 3303–3310.
[14] T. Yamanari, T. Taima, J. Sakai, J. Tsukamoto, Y. Yoshida, Effect of buffer layers on stability of polymer-based organic solar cells, Jpn. J. Appl. Phys. 49 (1) (2010) 01AC02.
[15] M.O. Reese, A.J. Morfa, M.S. White, N. Kopidakis, S.E. Shaheen, G. Rumbles, D.S. Ginley, Pathways for the degradation of organic photovoltaic P3HT: PCBM based devices, Sol. Energy Mater. Sol. Cells 92 (7) (2008) 746–752.
[16] L.M. Do, E.M. Han, Y. Niidome, M. Fujihira, T. Kanno, S. Yoshida, A. Maeda, A. J. Ikushima, Observation of degradation processes of Al electrodes in organic electroluminescence devices by electroluminescence microscopy, atomic force microscopy, scanning electron microscopy, and Auger electron spectroscopy, J. Appl. Phys. 76 (9) (1994) 5118.
[17] L.-M. Do, M. Oyamada, A. Koike, E.-M. Han, N. Yamamoto, M. Fujihira, Morphological change in the degradation of Al electrode surfaces of electroluminescent devices by fluorescence microscopy and AFM, Thin Solid Films 273 (1–2) (1996) 209–213.
[18] V.N. Savvate'ev, A.V. Yakimov, D. Davidov, R.M. Pogreb, R. Neumann, Y. Avny, Degradation of nonencapsulated polymer-based light-emitting diodes: noise and morphology, Appl. Phys. Lett. 71 (23) (1997) 3344.
[19] P. Favia, E. Voroshazi, P. Heremans, H. Bender, Investigation of aged organic solar cell stacks by cross-sectional transmission electron microscopy coupled with elemental analysis, J. Mater. Sci. 48 (7) (2013) 2908–2919.
[20] N. Rujisamphan, F. Deng, R.E. Murray, C. Ni, S. Ismat Shah, Focused ion beam assisted investigations of Al interface in polythiophene: fullerene solar cells, Sol. Energy Mater. Sol. Cells 109 (2013) 56–62.
[21] D.J. McClure, N. Copeland, Evaporated aluminum on polyester: optical, electrical, and barrier properties as a function of thickness and time (Part II), in: Proceedings of AIMCAL Fall Technical Conference, 2010.
[22] G. Kaune, E. Metwalli, R. Meier, V. Korstgens, K. Schlage, S. Couet, R. Rohlsberger, S.V. Roth, P. Muller-Buschbaum, Growth and morphology of sputtered aluminum thin films on P3HT surfaces, ACS Appl. Mater. Interfaces 3 (4) (2011) 1055–1062.
[23] M.T. Lloyd, D.C. Olson, P. Lu, E. Fang, D.L. Moore, M.S. White, M.O. Reese, D. S. Ginley, J.W.P. Hsu, Impact of contact evolution on the shelf life of organic solar cells, J. Mater. Chem. 19 (41) (2009) 7638.
[24] K. Norrman, F.C. Krebs, Lifetimes of organic photovoltaics: using TOF-SIMS and 18O2 isotopic labelling to characterise chemical degradation mechanisms, Sol. Energy Mater. Sol. Cells 90 (2) (2006) 213–227.
[25] K. Norrman, S.A. Gevorgyan, F.C. Krebs, Water-induced degradation of polymer solar cells studied by H218O labeling, ACS Appl. Mater. Interfaces 1 (1) (2008) 102–112.
[26] K. Feron, T.J. Nagle, L.J. Rozanski, B.B. Gong, C.J. Fell, Spatially resolved photocurrent measurements of organic solar cells: tracking water ingress at edges and pinholes, Sol. Energy Mater. Sol. Cells 109 (2013) 169–177.
[27] E. Voroshazi, B. Verreet, A. Buri, R. Müller, D. di Nuzzo, P. Heremans, Influence of cathode oxidation via the hole extraction layer in polymer: fullerene solar cells, Org. Electron. 12 (5) (2011) 736–744.
[28] H. Klumbies, M. Karl, M. Hermenau, R. Rösch, M. Seeland, H. Hoppe, L. Müller-Meskamp, K. Leo, Water ingress into and climate dependent lifetime of organic photovoltaic cells investigated by calcium corrosion tests, Sol. Energy Mater. Sol. Cells 120 (2014) 685–690.
[29] S. Schubert, H. Klumbies, L. Müller-Meskamp, K. Leo, Electrical calcium test for moisture barrier evaluation for organic devices, Rev. Sci. Instrum. 82 (9) (2011) 094101.
[30] H. Yi, S. Al-Faifi, A. Iraqi, D.C. Watters, J. Kingsley, D.G. Lidzey, Carbazole and thienyl benzo[1,2,5]thiadiazole based polymers with improved open circuit voltages and processability for application in solar cells, J. Mater. Chem. 21 (35) (2011) 13649–13656.
[31] D.R. Lide, Handbook of Chemistry and Physics, 72nd edition,. CRC Press, 1991.
[32] M.H.F. Overwijk, F.C. van den Heuvel, C.W.T. BulleLieuwma, Novel scheme for the preparation of transmission electron microscopy specimens with a focused ion beam, J. Vac. Sci. Technol. B 11 (6) (1993) 2021–2024.
[33] E.O. Hall, The deformation and ageing of mild steel: III. Discussion of results, Proc. Phys. Soc. Sect. B 64 (9) (1951) 747–753.
[34] N.J. Petch, The cleavage strength of polycrystals, J. Iron Steel Inst. 174 (1953) 25–28.
[35] S.R. Cowan, A. Roy, A.J. Heeger, Recombination in polymer-fullerene bulk heterojunction solar cells, Phys. Rev. B 82 (24) (2010).
[36] W.L. Leong, S.R. Cowan, A.J. Heeger, Differential resistance analysis of charge carrier losses in organic bulk heterojunction solar cells: observing the transition from bimolecular to trap-assisted recombination and quantifying the order of recombination, Adv. Energy Mater. 1 (4) (2011) 517–522.